



Synergistically creating sulfur vacancies in semimetal-supported amorphous MoS₂ for efficient hydrogen evolution



Guowei Li^{a,*}, Chenguang Fu^a, Jiquan Wu^b, Jiancun Rao^c, Sz-Chian Liou^c, Xijin Xu^d, Baiqi Shao^e, Kai Liu^e, Enke Liu^f, Nitesh Kumar^a, Xianjie Liu^b, Mats Fahlman^b, Johannes Gooth^a, Gudrun Auffermann^a, Yan Sun^a, Claudia Felser^a, Baomin Zhang^{d,*}

^a Max Planck Institute for Chemical Physics of Solids, 01187 Dresden, Germany

^b Department of Physics, Chemistry and Biology (IFM), Linköping University, 58183 Linköping, Sweden

^c AIM Lab, Maryland NanoCenter, University of Maryland, MD 20742 USA

^d School of Physics and Technology, University of Jinan, 250022 Jinan, China

^e Changchun Institute of Applied Chemistry, Chinese Academy of Sciences, 130022 Changchun, China

^f Institute of Physics, Chinese Academy of Sciences, 100190 Beijing, China

ARTICLE INFO

Keywords:

MoS₂
Sulfur vacancies
Electrocatalyst
Semimetal

ABSTRACT

The presence of elemental vacancies in materials are inevitable according to statistical thermodynamics, which will decide the chemical and physical properties of the investigated system. However, the controlled manipulation of vacancies for specific applications is a challenge. Here we report a facile method for creating large concentrations of S vacancies in the inert basal plane of MoS₂ supported on semimetal CoMoP₂. With a small applied potential, S atoms can be removed in the form of H₂S due to the optimized free energy of formation. The existence of vacancies favors electron injection from the electrode to the active site by decreasing the contact resistance. As a consequence, the catalytic current is increased by 221% with the vacancy-rich MoS₂ as electrocatalyst for hydrogen evolution reaction (HER). A small overpotential of 75 mV is needed to deliver a current density of 10 mA cm⁻², which is considered among the best values achieved for MoS₂. It is envisaged that this work may provide a new strategy for utilizing the semimetal phase for structuring MoS₂ into a multi-functional material.

1. Introduction

The elemental vacancies in materials, which are generally called defects, are actually considered to be perfect and powerful tools for designing various functional materials [1–4]. The vacancies can be viewed as virtual atoms that have an empty electronic state at the vacuum level, and thus the charge imbalances will lead to the redistribution of charges and consequently induce defect levels in the band gap, resulting in a richness of phenomena such as band gap narrowing, band bending, and symmetry distortion [5–7]. As a typical two-dimensional (2D) material, MoS₂ provides an ideal prototype to explore the interaction between vacancies and functions, especially in the field of electrochemical water splitting [8–13]. It has been clearly proven that the edge sites are catalytically active, while the basal plane is pretty inert [14]. Recent work demonstrated that sulfur vacancies could serve as another important catalytically active site for HER due to the favorable adsorption free energy [15,16]. This is supported by the

theoretical calculations of the formation energy of S vacancies, which is much lower than that of Mo vacancies. The major result is the emergence of impurity states in the bandgap that allow favorable hydrogen adsorption [17–19].

However, the controlled fabrication of S vacancies in the inert plane of MoS₂ is a formidable challenge and generally needs critical conditions such as electron/argon irradiation, hydrogen plasma treatment, or high temperature annealing [20,21]. A recent work reported the possibility of creating S vacancies in the electrochemical process but need a large accessible applied potential. This is understandable because removal of S by H₂ to release H₂S is very endothermic and kinetically difficult to achieve [22,23]. Recent work found that the robust electronic states on topological insulators could enhance the adsorption of various molecular species when covered by selected catalytic metal layers [24]. Informed by the deposition of oxide thin films on the substrate, where oxygen vacancies can be formed due to the strong affinity between oxygen and the element from the substrate [25], it is

* Corresponding authors.

E-mail addresses: Guowei.li@cpfs.mpg.de (G. Li), sps_zhangbm@ujn.edu.cn (B. Zhang).

very interesting to explore the synergistic effect on the formation of S vacancies in the semimetal phase – supported MoS₂.

As a recent defined semimetal, CoMoP₂ is selected as the supporting substrate because of the good conductivity and similar hexagonal structure as MoS₂ [26]. Density functional theory (DFT) calculation predicted that the S atoms in the basal plane could be activated and removed by bonding with hydrogen. The formation energy barrier for H₂S was significantly decreased in comparison with the pure MoS₂ phase without support. S vacancies with a concentration of 13% could be created in the electrochemical process. Consequently, the catalytic current was increased by 221% at a given overpotential (-0.25 V vs RHE) and show high stability in a wide potential window. This opens new pathways for the ready creation of vacancies in 2D materials for various applications.

2. Experimental

2.1. Synthesis of the catalysts

The topological semimetal CoMoP₂ was synthesized by solid state reaction. In a typically synthesis, 0.25 mmol NH₄Mo₇O₂₄·4H₂O, 1.75 mmol Co(NO₃)₂·6H₂O, 4 mmol (NH₄)₂HPO₄, 4 mmol citric acid, and 2.5 g urea were dissolved in distilled water. Then solution was dried at 80 °C and then heated at 500 °C for 4 h in the air. After this, it was moved into a tube furnace and heated at 850 °C for 2 h with a heating rate of 1 °C/min. Hydrogen flow was used in this process.

For the synthesis of MoS₂/CoMoP₂ heterostructure (CMPS), 50 mg of the as-synthesized powder, 50 mg of (NH₄)₂MoS₄, and a Ni foam were placed in a 50 mL autoclave filled with 20 mL of *N,N*-Dimethylformamide. 0.1 mL of N₂H₄ H₂O was added drop by drop. The mixed solution was transferred into an oven and heated at 180 °C for 24 h. The produced product was washed with water first and then with ethanol, and dried at 60 °C for the following characterization.

2.2. Characteristic techniques and electrochemical activation strategy

Powder X-ray diffraction (XRD) data were recorded with a Bruker D8 Advance diffractometer equipped with a Cu K α source ($\lambda = 0.15406$ nm). The morphologies and structures of the products were characterized with TITAN 80/300 electron microscope. XPS investigation was carried on a UHV surface analysis system equipped with a Scienta-200 hemispherical analyzer. The base pressure of a sample analysis chamber is 2×10^{-10} mbar.

Electrochemical activation and performance assessment were performed on the Autolab PGSTAT302N with impedance module electrochemistry workstation. A conventional three electrode cell configuration was employed. The Ni foam with pristine CMPS sample were used directly as working electrode. A Ag/AgCl (3 M KCl) electrode was used as the reference electrode, and a graphite rod was used as the counter electrode. 1 M KOH was used as electrolyte. Linear sweep voltammetry was recorded at a scan rate of 1 mV/s. All the polarization curves were iR-corrected by electrochemical impedance spectroscopy (EIS). The solution resistance (Rs) was estimated from the impedance at high frequency ($|Z(j\omega)|\omega \rightarrow \infty$). The activation process was performed in potentiostatic mode at -0.126 V vs RHE for 40 h. All the potentials reported in this work were converted to a reversible hydrogen electrode according to E (versus RHE) = E (versus Ag/AgCl) + (0.207 + 0.059 pH) V.

2.3. Theoretical calculations

The crystal structure of CoMoP₂ is fully relaxed (including the shape and the volume of the unit cell, and the internal positional parameters), and the optimized lattice parameters agree well with experimental values within a discrepancy of 0.5%. The optimized lattice parameters of CoMoP₂ in a-b plane were used to construct the basic unit of the

supercell in a-b plane. Taking account of the necessity of creating S vacancies in supercells and the acceptable computational efforts of DFT methods when treating vacancies in solids, in a-b plane, the dimension of the supercell is chosen to be 4*4 basic units of CoMoP₂. The heterostructure is constructed by adding one monolayer of 2H-MoS₂ on top of the Co-terminated CoMoP₂ (001) surface. All calculations on supercells in this work are based on the slab model, and the thickness of the vacuum region is chosen to be as large as 12 Å in order to reduce the mirror image effect to a negligible value. In this work, we keep the shape and the volume of supercells fixed, optimize the internal positional parameters of supercells only, and keep the Co atomic layer at the bottom of each supercell fixed mimicking the CoMoP₂ substrate.

3. Results and discussions

3.1. Theoretical prediction of S vacancy formation

To explore why and how S vacancies are formed, we first performed DFT calculations of the surface free energies on three different supercells: (a) In the case with one S atom adsorbed on the S vacancy (denoted as \square S, which can also be called pristine MoS₂/CoMoP₂ heterostructure (CMPS), as shown in Fig. S1a); (b) In the case with one S vacancy (denoted as Mo \square S_x/CoMoP₂, as shown in Fig. S1b), and (c) For the case with one H adsorbed on the S vacancy (denoted as Mo \square S_x(H)/CoMoP₂, as shown in Fig. S1c). As shown in Fig. 1b, the surface energy of Mo \square S_x/CoMoP₂ is larger than that of pristine structure, until the potential of as low as -1.26 V vs RHE. This is inconsistent with previous research, which indicated that in spite of perfect 2D materials such as MoS₂, being predicted to be unstable upon thermal fluctuation [27], the creation of vacancies in the basal plane is reasonably difficult [28]. However, once created, they can be occupied immediately by hydrogen atoms under the electrochemical conditions in a broad potential window below 0.42 V vs RHE as illustrated by the arrow in Fig. 1b. This value is much higher than that of pure MoS₂ phase, with a value of -0.26 V vs RHE [22]. This readily explains the instability of S vacancies because they can be easily passivated by adsorbates [29]. Obviously, the vacancies created while supported on semimetal CoMoP₂ are more stable than the pure MoS₂ phase. We then calculated the Gibbs free energy for H₂S, which is the desulfurization process of making S vacancies. This is a two proton-electron transfer process, as shown in Fig. 1a and b. The transfer of the first electron and proton needs an energy of 1.43 eV, while the second protonation to form adsorbed H₂S is uphill by about 1.51 eV from the first step. However, the whole reaction becomes exergonic with an absolute applied potential in the electrochemical environment. The ΔG for formation of gaseous H₂S was decreased to only 0.08 eV for the MoS₂/CoMoP₂ heterostructure, which is much lower than that for pure MoS₂ with a value of -0.83 eV. This means that the S can be removed more efficiently as H₂S gas and serves as activity centers in the following HER process.

3.2. Catalyst structure and composition

Based on the calculations, we constructed the hybrid structure by a two-step process as illustrated in Fig. 1d. CoMoP₂ nanoparticles were synthesized first by the in-situ reduction of Co-Mo complex precursor at high temperature under H₂ flow. Then, the pristine MoS₂ was directly grown on a Ni foam in the solution containing CoMoP₂ nanoparticles and ammonium thiomolybdate ((NH₄)₂MoS₄). As revealed in the X-ray diffraction pattern (Fig. 2a), the main peaks can be assigned to the hexagonal phase of CoMoP₂ with a space group *P6₃/mmc*, No.194 ($a = 0.333$ nm, $c = 1.122$ nm). The absence of diffraction peaks of MoS₂ prove that the obtained pristine phase is amorphous. Fig. 2b shows the Scanning electron microscope (SEM) image of the final structure, with MoS₂/CoMoP₂ particles grown on the Ni foam. The corresponding energy-dispersive X-ray spectroscopy (EDS) analysis confirmed the particle is composed of the elements Mo, S, Co, and P

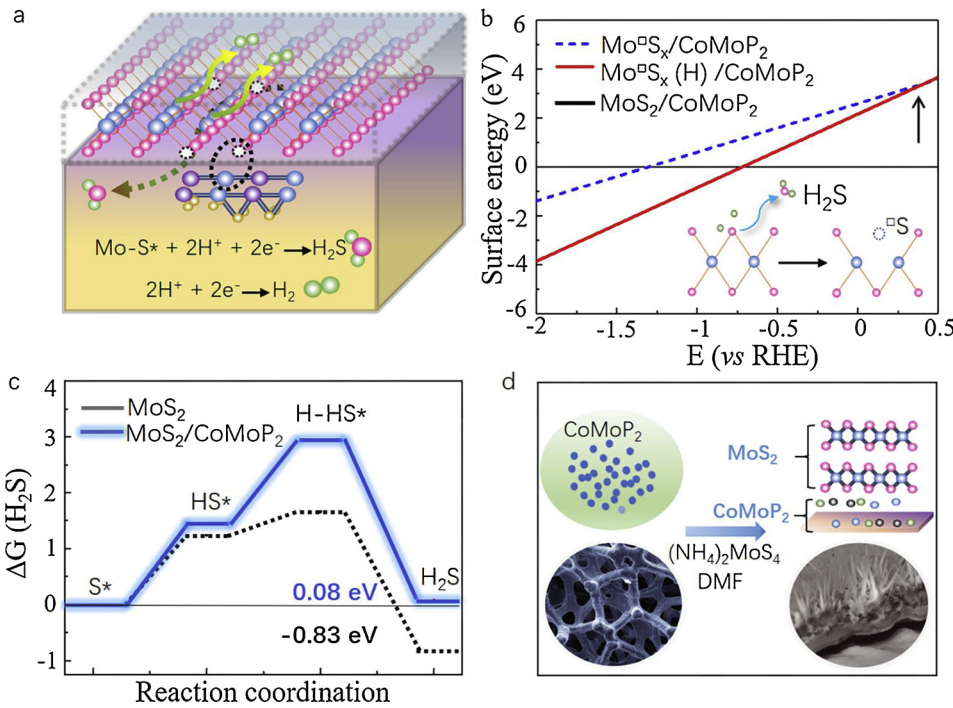


(Fig. 2b), which were distributed homogeneously according to elemental mapping (Fig. S2). High-resolution transmission electron microscopy (HRTEM) further confirmed the crystallinity and composition of the as-synthesized hybrid structure. Several nanoparticles are covered by a thick layer of amorphous shell (Fig. 2c), but one can observe some tiny layered structures at the edge with a lattice fringe spacing of ~0.6 nm, corresponding to the (002) facet of bulk 2H-MoS₂ (Fig. 2d), indicating the formation of a few crystalline nuclei from the amorphous matrix [30]. The lattice-resolved image of a single crystalline domain embedded in the amorphous matrix has an interplanar spacing of 0.19 nm, which corresponds to the (114) plane of hexagonal CoMoP₂

phase (Fig. 2e). This is consistent with the fast-Fourier transform (FFT) image that recorded along the [221] direction (Fig. 2f).

3.3. Electrochemical activation and HER performance

The electrochemical activation process of the pristine MoS₂ for HER was conducted in 1 M KOH solution in a standard three-electrode electrochemical cell. All the LSV curves displayed in this work are corrected to remove the iR drop by electrochemical impedance spectroscopy (EIS). At the current density of 10 mA/cm², Pt/C and bare Ni foam exhibited HER overpotentials of 26 mV and 200 mV, respectively

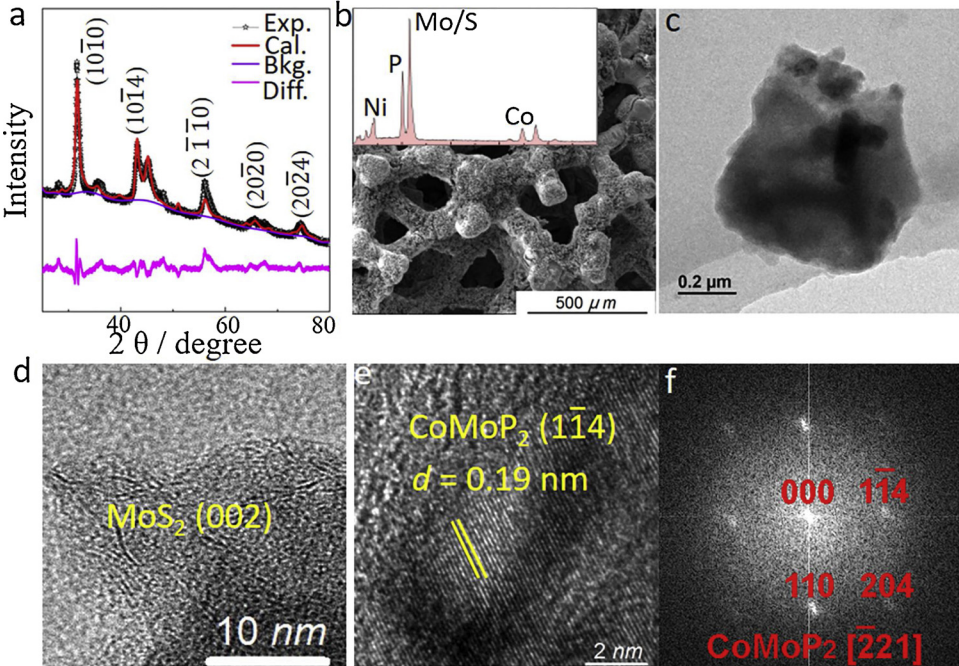
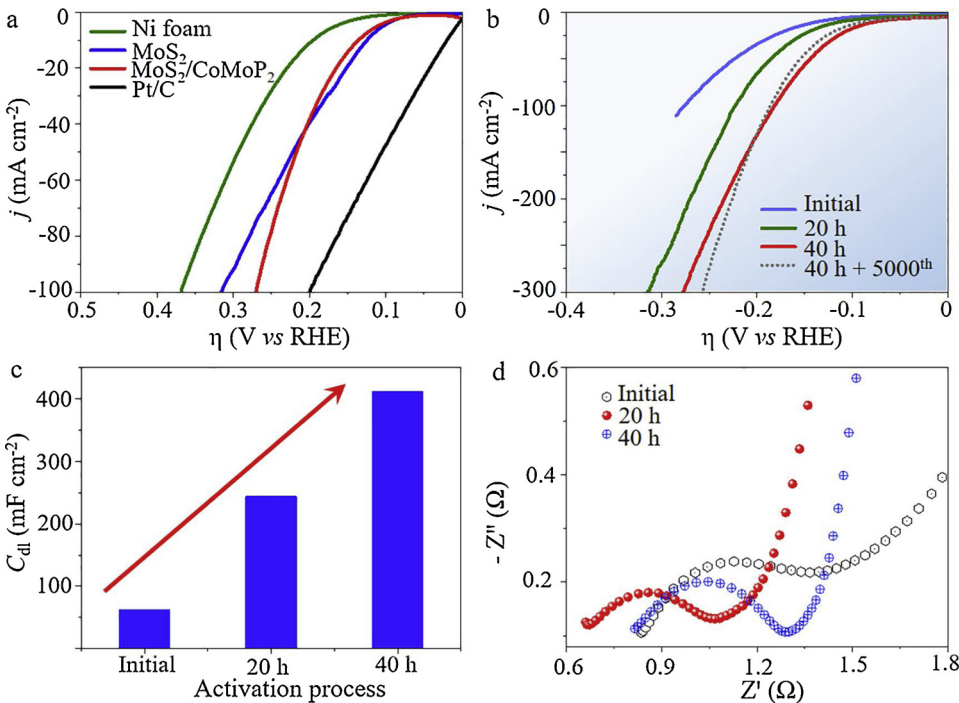


Fig. 2. (a) The XRD pattern of the synthesized MoS₂/CoMoP₂ sample. (b) SEM and (c) TEM image of the MoS₂/CoMoP₂ particle. (d) HRTEM shows the low crystalline MoS₂ phase outside, and (e). Semimetal CoMoP₂ phase inside, and (f). The corresponding fast Fourier transform (FFT).



(Fig. 3a). The HER activity of the pure MoS₂ and pristine CMPS are roughly the same, which is 116 and 126 mV, respectively. Furthermore, the linear parts of the polarization curves were fitted by the Tafel equation, yielding Tafel slopes of 30, 109, 67, and 80 mV/dec. for commercial Pt/C, Ni foam, bare MoS₂, and pristine CMPS samples, respectively (Fig. S3). These results indicate that the pure MoS₂ and pristine CMPS have the similar HER activities during the initial measurements. Then, a long-term stability test was carried out on the pristine CMPS sample with a constant overpotential of 126 mV without *iR* corrections (Fig. S4). Interestingly, instead of remaining unchanged or exhibiting degradation in current densities with increasing measurement time, we found a continuously increasing current density. The polarization curve was recorded after 20 h of measurement, as shown in Fig. 3b. The overpotential to deliver a current density of 10 mA/cm² is decreased to 110 mV. For a meaningful comparison, a normalized current density increment is defined as $\Delta J/J_0$, where J_0 is the current density of pristine CMPS, and ΔJ is the current density increase at -0.25 V [22]. This value was determined to be 115% after 20 h, and it increased to 221% after another 20 h of further testing. Impressively, the overpotential to produce a current density of 10 mA/cm² is only ~75 mV after activation. This value is better than most reported MoS₂ based catalysts (Table S1), such as CoS-doped β -Co(OH)₂@amorphous MoS_{2+x} hybrid (143 mV) [31], MoS₂/Ni₃S₂ heterostructures (110 mV) [32], MoS₂/NiCo-layered double hydroxide (78 mV) [33], and metallic-phase MoS₂ nanosheets (175 mV) [34]. Furthermore, the polarization curve after 40 h plus 5000 cycling test are compared in Fig. 3b. The minuscule difference in current density suggests a high long-term stability of our vacancy-rich catalyst in the HER process.

To confirm the increase of active centers, the active surface areas of the catalyst before and after activation were analyzed by their electrochemical double layer capacitances (C_{dl}) (Figs. S5–S7). As shown in 3a, the C_{dl} increased dramatically from 62.1 to 244 m F cm⁻² after 20 h activation, and finally to 412 m F cm⁻² after 40 h, illustrating that the increase in catalytic current can be attributed to the increased electrochemical surface area of MoS₂. Electrochemical impedance spectroscopy (EIS) was performed under the HER conditions (Fig. 3d). The EIS plots can be fitted excellent by two-time constant serial (2TS) model. The semicircle at high frequency (HF) can be assigned to the charge transfer kinetics from catalyst to adsorbates. The charge transfer

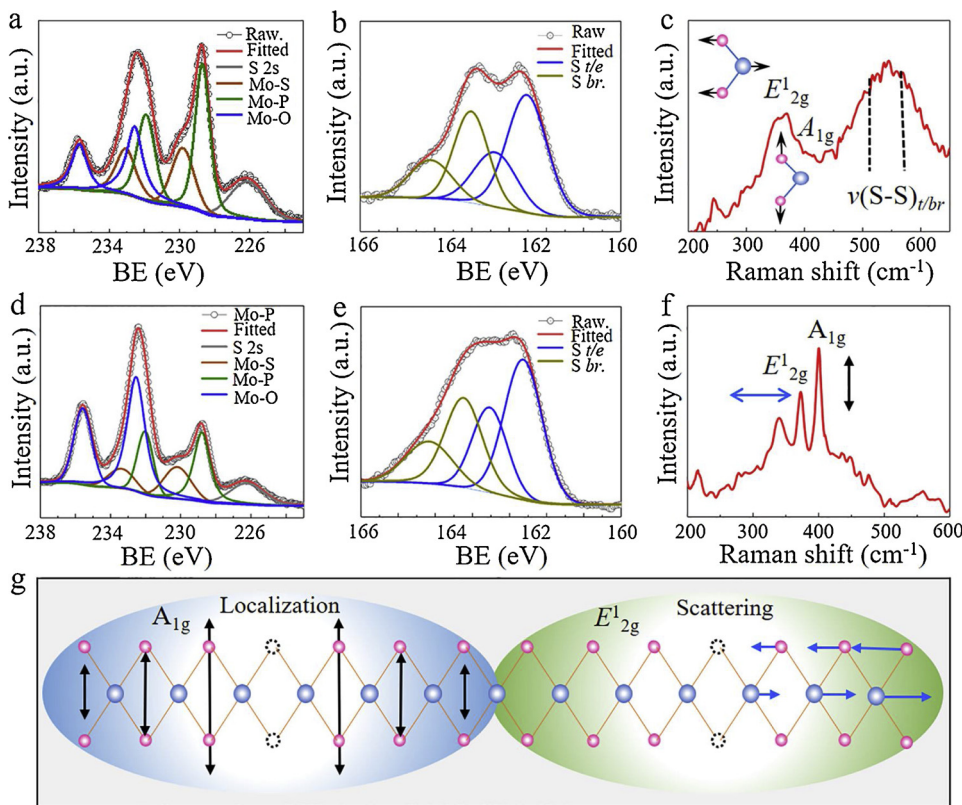
Fig. 3. (a) Polarization curves of Ni foam (NF), pure MoS₂ phase, commercial Pt/C catalyst, and pristine MoS₂/CoMoP₂. (b) Comparison of polarization curves for the MoS₂/CoMoP₂ catalyst in the initial test, and after activation for 20 h, 40 h, and 40 h plus 5000 cycles. (c) Plot showing the increase of double-layer capacitance (C_{dl}) for the pristine and vacancy-rich MoS₂/CoMoP₂ sample for the initial test, activated for 20 h, and 40 h, respectively. (d) Impedance measurement of the pristine MoS₂/CoMoP₂ and activated for 20 and 40 h, respectively.

resistance is decreased from 4.8Ω to 3.2Ω after 20 h activation, and further decreased to 2.6Ω after 40 h. Bode phase diagram clearly reveals the relaxation time at HF as shown Fig. S8. After catalyst activation, the intensities of HF semicircle decrease and shift to higher frequencies, indicating an increase in the reaction rate and shorter reaction time constant ($\tau = 1/\omega_p$, where τ is the time constant and ω_p is the characteristic frequency). This indicates an increase in the number of edge-terminated states or vacancy states that were acting as catalytic centers, which favors electron injection in the HER process. Previous studies found that metal phosphides such as MoP and CoP are also excellent electrocatalysts for HER [35,36]. Thus, as a comparison, pure MoS₂, CoMoP₂, and Ni foam were tested further proving the activation process. The results showed a stable performance without activation from the LSV curves (Figs. S9–S11). All these suggest that the using of CoMoP₂ substrate is very important for the activation process.

Finally, we tried to investigate the HER behavior under acidic condition. Surprisingly, there was no obvious activation happened from the LSV curves (Fig. S12). This maybe caused by the presence of large number of protons in acidic solution. The Volmer process for HER has a smaller Gibbs free energy than that of S-vacancy formation. Thus, rather than the formation of H₂S gas, hydrogen atoms are reduced to forming hydrogen gas.

3.4. Catalyst structure evolution before and after electrochemical activation

The phase structure, as well as the formation of S vacancies were examined by X-ray photoelectron spectroscopy (XPS). For the pristine MoS₂/CoMoP₂ sample, a small S 2s peak (226.1 eV) next to the Mo 3 d_{5/2} peak was observed (Fig. 4a) [37,38]. Specifically, these doublets with binding energies of 228.6/231.9 eV can be assigned to the Mo 3d signal of Mo-P bonding in CoMoP₂ (Fig. 4a). The peaks located at 229.8 and 233.1 eV with a separation of 3.3 eV can be attributed to the Mo species in MoS₂ phase [39,40]. Moreover, the Mo 3d peaks at higher binding energies (232.5 eV and 235.7 eV) demonstrate slight surface oxidation of the pristine MoS₂ surface into MoO₃ [41]. The S 2p peak, on the other hand, can be best fitted with two doublets of S 2p_{3/2} energy states (Fig. 4b). The binding energy of 161.5 eV corresponds to the terminal (edge) site of S²⁻ species, which have been identified clearly as active sites for the HER catalytic activity in MoS₂ [15]. The higher binding



energy at 163 eV can be assigned to the bridging disulfide S_2^{2-} ligand or apical S^{2-} ligand [42,43]. The atomic ratio between S and Mo is determined to be ~2 by the above fitting results. Further insight into the pristine MoS_2 nanostructure was obtained by examination of Raman spectrum (Fig. 4c). The broad peak between 350–420 cm^{-1} belongs to the E_{2g}^1 (in plane motion of Mo and S in opposite directions) and A_{1g} (out of plane motions of S atoms) vibrational modes of hexagonal MoS_2 phase, respectively. Of particular note is the dramatically decrease in the relative intensities of A_{1g} to E_{2g}^1 in comparison with the bulk phase, suggesting that the as-prepared MoS_2 structure is edge-poor [30,39]. This readily explains the poor initial HER activity as discussed below. Another broad peak centered at 543 cm^{-1} is a feature of the amorphous MoS_2 phase, which can be assigned to the $\nu(\text{S}-\text{S})_{\text{terminal}}$ and $\nu(\text{S}-\text{S})_{\text{bridging}}$ vibrations [44,45].

In comparison with the pristine sample, the binding energies for Mo–O and Mo–P bonding remained unchanged (Fig. 4d) after activation. The increase in the peak density of Mo–O bonding (232.5 eV) can be explained by surface oxidation, as observed in other systems. Interestingly, the full width at half maximum of the Mo–S peak was larger than that of the pristine sample, and the binding energy shifted to a lower position by 0.11 eV. This means the element Mo has different S coordination and lower valence states should exist after activation. The investigation of S 2p spectra indicates that the intensity was significantly reduced after compared to the Mo 3d peak, while the relative intensity of terminal/edge S was increased by comparison with basal bridging component (Fig. 4e). The atomic ratio between S and Mo was decreased to 1.73 by fitting the spectra, corresponding to a S vacancy concentration of 13%. All these suggest the creation of S vacancies after activation, which serves as active centers for HER [46]. More evidence was provided by the Raman spectra, as shown in Fig. 4f. The strong A_{1g} peak reveals that the out of plane vibration is favored, suggests in the increasing of terminal/edge-terminated component [30,39]. The red shift of A_{1g} (401 cm^{-1}) to E_{2g}^1 (372 cm^{-1}) in comparison with the bulk phase was the result of increases in disorder associated with edge defects [47,48]. Additionally, a satellite peak was observed beside the E_{2g}^1

Fig. 4. (a). XPS spectra of Mo 3d peak, and (b). S 2p peak, for the pristine $\text{MoS}_2/\text{CoMoP}_2$ sample. (c). Raman spectrum of the pristine $\text{MoS}_2/\text{CoMoP}_2$. XPS spectra of (d). Mo 3d peak, and (e). S 2p peak, for the activated $\text{MoS}_2/\text{CoMoP}_2$ sample. (f). Raman spectrum of the $\text{MoS}_2/\text{CoMoP}_2$ after activation. (g). An illustration of the function of S vacancies as localization and scattering centers for Raman vibration.

mode, sitting at smaller wavenumbers of 341 cm^{-1} . This further positively confirms that the defects are from S vacancies as expected from previous theoretical predication: the S vacancy could be the localization centers for out of plane vibration and strengthen the A_{1g} mode, while acting as scattering centers for in-plane vibration (E_{2g}^1 mode) and causing the atoms around the vacancies to have a smaller vibrational amplitude (Fig. 4g) [49,50].

4. Conclusions

In conclusion, large concentrations of S vacancies were created in the basal plane of MoS_2 when supported on the topological semimetal CoMoP_2 . Structural characterization revealed that the created vacancies can serve as new catalytic centers for HER and are related to the increase in catalytic current by more than a factor of two, and the efficient electron injection from the electrode to the catalyst. DFT calculations further confirmed these results by revealing a significant decrease in the Gibbs free energy for H_2S in the electrochemical process. This synergistic approach could not only be used to design high performance HER catalysts, but also provides a general strategy to creating vacancies for various applications.

Acknowledgements

The authors gratefully acknowledge Dr. Anil Kumar for the PXRD measurements. We would also like to thank Dr. Qianan Xu for the helpful discussions. This work was financially supported by the European Research Council (ERC Advanced Grant No. 291472'Idea Heusler') and ERC Advanced Grant (No. 742068). TOPMAT'. B. Zhang thank the support of the Natural Science Foundation of Shandong Province (CN) with Grants No. ZR2016AB12.

Appendix A. Supplementary data

Supplementary material related to this article can be found, in the

online version, at doi:<https://doi.org/10.1016/j.apcatb.2019.04.080>.

References

- [1] C. Ran, J. Xu, W. Gao, C. Huang, S. Dou, Defects in metal triiodide perovskite materials towards high-performance solar cells: origin, impact, characterization, and engineering, *Chem. Soc. Rev.* 47 (2018) 4581–4610.
- [2] D.A. Tompsett, S.C. Parker, M.S. Islam, Rutile (beta-)MnO₂ surfaces and vacancy formation for high electrochemical and catalytic performance, *J. Am. Chem. Soc.* 136 (2014) 1418–1426.
- [3] G. Li, B. Zhang, J. Rao, D. Herranz Gonzalez, G.R. Blake, R.A. de Groot, T.T.M. Palstra, Effect of vacancies on magnetism, electrical transport, and thermoelectric performance of marcasite FeSe_{2-δ}(δ = 0.05), *Chem. Mater.* 27 (2015) 8220–8229.
- [4] D. Ruan, S. Kim, M. Fujitsuka, T. Majima, Defects rich g-C₃N₄ with mesoporous structure for efficient photocatalytic H₂ production under visible light irradiation, *Appl. Catal. B-Environ.* 288 (2018) 638–646.
- [5] J.M. Wu, Y. Chen, L. Pan, P.H. Wang, Y. Cui, D.C. Kong, L. Wang, X.W. Zhang, J.J. Zou, Multi-layer monoclinic BiVO₄ with oxygen vacancies and V⁴⁺ species for highly efficient visible-light photoelectrochemical applications, *Appl. Catal. B-Environ.* 221 (2018) 187–195.
- [6] X. Li, T. Li, Y. Ma, Q. Wei, W. Qiu, H. Guo, X. Shi, P. Zhang, A.M. Asiri, L. Chen, B. Tang, X. Sun, Boosted electrocatalytic N₂ reduction to NH₃ by defect-rich MoS₂ nanoflower, *Adv. Energy Mater.* 8 (2018) 1801357.
- [7] G. Li, G.R. Blake, T.T. Palstra, Vacancies in functional materials for clean energy storage and harvesting: the perfect imperfection, *Chem. Soc. Rev.* 46 (2017) 1693–1706.
- [8] U. Gupta, C.N.R. Rao, Hydrogen generation by water splitting using MoS₂ and other transition metal dichalcogenides, *Nano Energy* 41 (2017) 49–65.
- [9] H. Wang, Z. Lu, S. Xu, D. Kong, J.J. Cha, G. Zheng, P.C. Hsu, K. Yan, D. Bradshaw, F.B. Prinz, Y. Cui, Electrochemical tuning of vertically aligned MoS₂ nanofilms and its application in improving hydrogen evolution reaction, *Proc. Natl. Acad. Sci.* 110 (2013) 19701–19706.
- [10] P.S. Maiti, A.K. Ganai, R. Bar-Ziv, A.N. Enyashin, L. Houben, M.B. Sadan, Cu_{2-x}S-MoS₂ nano-octahedra at the atomic scale using a template to activate the basal plane of MoS₂ for hydrogen production, *Chem. Mater.* 30 (2018) 4489–4492.
- [11] S. Chen, X. Chen, G. Wang, L. Liu, Q. He, X.-B. Li, N. Cui, Reaction mechanism with thermodynamic structural screening for electrochemical hydrogen evolution on monolayer 1T' phase MoS₂, *Chem. Mater.* 30 (2018) 5404–5411.
- [12] Y.Z. Liu, X.Y. Xu, J.Q. Zhang, H.Y. Zhang, W.J. Tian, X.J. Li, M.O. Tade, H.Q. Sun, S.B. Wang, Flower-like MoS₂ on graphitic carbon nitride for enhanced photocatalytic and electrochemical hydrogen evolutions, *Appl. Catal. B-Environ.* 239 (2018) 334–344.
- [13] J. Liu, Y. Liu, D. Xu, Y. Zhu, W. Peng, Y. Li, F. Zhang, X. Fan, Hierarchical nanoroll like MoS₂Ti₃C₂T_x hybrid with high electrocatalytic hydrogen evolution activity, *Appl. Catal. B-Environ.* 241 (2019) 89–94.
- [14] T.F. Jarillo, K.P. Jorgensen, J. Bonde, J.H. Nielsen, S. Horsch, I. Chorkendorff, Identification of active edge sites for electrochemical H₂ evolution from MoS₂ nanocatalysts, *Science* 317 (2007) 100–102.
- [15] G. Li, D. Zhang, Q. Qiao, Y. Yu, D. Peterson, A. Zafar, R. Kumar, S. Curtarolo, F. Hunte, S. Shannon, Y. Zhu, W. Yang, L. Cao, All the catalytic active sites of MoS₂ for hydrogen evolution, *J. Am. Chem. Soc.* 138 (2016) 16632–16638.
- [16] T.A. Ho, C. Bae, S. Lee, M. Kim, J.M. Montero-Moreno, J.H. Park, H. Shin, Edge-on MoS₂ thin films by atomic layer deposition for understanding the interplay between the active area and hydrogen evolution reaction, *Chem. Mater.* 29 (2017) 7604–7614.
- [17] J. Hong, Z. Hu, M. Probert, K. Li, D. Lv, X. Yang, L. Gu, N. Mao, Q. Feng, L. Xie, J. Zhang, D. Wu, Z. Zhang, C. Jin, W. Ji, X. Zhang, J. Yuan, Z. Zhang, Exploring atomic defects in molybdenum disulphide monolayers, *Nat. Commun.* 6 (2015) 6293.
- [18] D. Liu, Y. Guo, L. Fang, J. Robertson, Sulfur vacancies in monolayer MoS₂ and its electrical contacts, *Appl. Phys. Lett.* 103 (2013) 183113.
- [19] H. Li, Charlie Tsai, Al Leen Koh, Lili Cai, Alex W. Contrynman, Alex H. Frapapane, Jiheng Zhao, Hyun Soo Han, Hari C. Manoharan, Frank Abild-Pedersen, Jens K. Nørskov, Xiaolin Zheng, Activating and optimizing MoS₂ basal planes for hydrogen evolution through the formation of strained sulphur vacancies, *Nat. Mater.* 15 (2016) 48–53.
- [20] Z. Yu, Y. Pan, Y. Shen, Z. Wang, Z.Y. Ong, T. Xu, R. Xin, L. Pan, B. Wang, L. Sun, J. Wang, G. Zhang, Y.W. Zhang, Y. Shi, X. Wang, Towards intrinsic charge transport in monolayer molybdenum disulfide by defect and interface engineering, *Nat. Commun.* 5 (2014) 5290.
- [21] S. Bertolazzi, S. Bonacchi, G. Nan, A. Pershin, D. Beljonne, P. Samori, Engineering chemically active defects in monolayer MoS₂ transistors via ion-beam irradiation and their healing via vapor deposition of alkanethiols, *Adv. Mater.* 29 (2017) 1606760.
- [22] C. Tsai, H. Li, S. Park, J. Park, H.S. Han, J.K. Nørskov, X. Zheng, F. Abild-Pedersen, Electrochemical generation of sulfur vacancies in the basal plane of MoS₂ for hydrogen evolution, *Nat. Commun.* 8 (2017) 15113.
- [23] S. Cristol, J.F. Paul, E. Payen, Theoretical study of the MoS₂ (100) surface: a chemical potential analysis of sulfur and hydrogen coverage, *J. Phys. Chem. B* 104 (2000) 11220–11229.
- [24] H. Chen, W. Zhu, D. Xiao, Z. Zhang, CO oxidation facilitated by robust surface states on Au-covered topological insulators, *Phys. Rev. Lett.* 107 (2011) 056804.
- [25] Z.Q. Liu, C.J. Li, W.M. Lü, X.H. Huang, Z. Huang, S.W. Zeng, X.P. Qiu, L.S. Huang, A. Annadi, J.S. Chen, J.M.D. Coey, T. Venkatesan, Ariando, Origin of the two-dimensional electron gas at LaAlO₃/SrTiO₃ interfaces: the role of oxygen vacancies and electronic reconstruction, *Phys. Rev. X* 3 (2013) 021010.
- [26] T. Zhang, Y. Jiang, Z. Song, H. Huang, Y. He, Z. Fang, H. Weng, C. Fang, Catalogue of topological electronic materials, *Nature* 566 (2019) 475–479.
- [27] Z. Lin, B.R. Carvalho, E. Kahn, R. Lv, R. Rao, H. Terrones, M.A. Pimenta, M. Terrones, Defect engineering of two-dimensional transition metal dichalcogenides, *2D Mater.* 3 (2016) 022002.
- [28] M.G. Sensoy, D. Vinichenko, W. Chen, C.M. Friend, E. Kaxiras, Strain effects on the behavior of isolated and paired sulfur vacancy defects in monolayer MoS₂, *Phys. Rev. B* 95 (2017) 014106.
- [29] H. Lu, A. Kummel, J. Robertson, Passivating the sulfur vacancy in monolayer MoS₂, *APL Mater.* 6 (2018) 066104.
- [30] M.R. Gao, M.K. Chan, Y. Sun, Edge-terminated molybdenum disulfide with a 9.4-A interlayer spacing for electrochemical hydrogen production, *Nat. Commun.* 6 (2015) 7493.
- [31] T. Yoon, K.S. Kim, One-step synthesis of CoS-Doped β-Co(OH)₂@Amorphous MoS_{2+x} hybrid catalyst grown on nickel foam for high-performance electrochemical overall water splitting, *Adv. Funct. Mater.* 26 (2016) 7386–7393.
- [32] J. Zhang, T. Wang, D. Pohl, B. Rellinghaus, R. Dong, S. Liu, X. Zhuang, X. Feng, Interface engineering of MoS₂/Ni₃S₂ heterostructures for highly enhanced electrochemical overall-water-splitting activity, *Angew. Chemie* 55 (2016) 6702–6707.
- [33] J. Hu, C. Zhang, L. Jiang, H. Lin, Y. An, D. Zhou, M.K.H. Leung, S. Yang, Nanohybridization of MoS₂ with layered double hydroxides efficiently synergizes the hydrogen evolution in alkaline media, *Joule* 1 (2017) 383–393.
- [34] X. Geng, W. Sun, W. Wu, B. Chen, A. Al-Hilo, M. Benamarra, H. Zhu, F. Watanabe, J. Cui, T.P. Chen, Pure and stable metallic phase molybdenum disulfide nanosheets for hydrogen evolution reaction, *Nat. Commun.* 7 (2016) 10672.
- [35] Z. Xing, Q. Liu, A.M. Asiri, X. Sun, Closely interconnected network of molybdenum phosphide nanoparticles: a highly efficient electrocatalyst for generating hydrogen from water, *Adv. Mater.* 26 (2014) 5702–5707.
- [36] J. Tian, Q. Liu, A.M. Asiri, X. Sun, Self-supported nanoporous cobalt phosphide nanowire arrays: an efficient 3D hydrogen-evolving cathode over the wide range of pH 0–14, *J. Am. Chem. Soc.* 136 (2014) 7587–7590.
- [37] J. Kibsgaard, T.F. Jarillo, Molybdenum phosphosulfide: an active, acid-stable, earth-abundant catalyst for the hydrogen evolution reaction, *Angew. Chemie* 53 (2014) 14433–14437.
- [38] L. Zhang, X. Ji, X. Ren, Y. Ma, X. Shi, Z. Tian, A.M. Asiri, L. Chen, B. Tang, X. Sun, Electrochemical ammonia synthesis via nitrogen reduction reaction on a MoS₂ catalyst: theoretical and experimental studies, *Adv. Mater.* 30 (2018) e1800191.
- [39] M.A.R. Anjum, H.Y. Jeong, M.H. Lee, H.S. Shin, J.S. Lee, Efficient hydrogen evolution reaction catalysis in alkaline media by all-in-One MoS₂ with multifunctional active sites, *Adv. Mater.* 30 (2018) e1707105.
- [40] J. Wang, J. Luo, D. Liu, S. Chen, T. Peng, One-pot solvothermal synthesis of MoS₂-modified Mn_{0.2}Cd_{0.8}SMn₃ heterojunction photocatalysts for highly efficient visible-light-driven H₂ production, *Appl. Catal. B* 241 (2019) 130–140.
- [41] G. Li, Y. Sun, J. Rao, J. Wu, A. Kumar, Q. Xu, C. Fu, E. Liu, R.G. Blake, P. Werner, B. Shao, K. Liu, S. Parkin, X. Liu, M. Fahlman, S.-C. Liou, G. Auffermann, J. Zhang, C. Felser, X. Feng, Carbon-tailored semimetal MoP as an efficient hydrogen evolution electrocatalyst in both alkaline and acid media, *Adv. Energy. Mater.* 8 (24) (2018) 1801258.
- [42] D. Dinda, M.E. Ahmed, S. Mandal, B. Mondal, S.K. Saha, Amorphous molybdenum sulfide quantum dots: an efficient hydrogen evolution electrocatalyst in neutral medium, *J. Mater. Chem. A Mater. Energy Sustain.* 4 (2016) 15486–15493.
- [43] Y. Li, K. Yin, L.L. Wang, X.L. Lu, Y.Q. Zhang, Y.T. Liu, D.F. Yan, Y.Z. Song, S.L. Luo, Engineering MoS₂ nanomesh with holes and lattice defects for highly active hydrogen evolution reaction, *Appl. Catal. B-Environ.* 239 (2018) 537–544.
- [44] Y. Deng, L.R.L. Ting, P.H.L. Neo, Y.-J. Zhang, A.A. Peterson, B.S. Yeo, Operando raman spectroscopy of amorphous molybdenum sulfide (MoS_x) during the electrochemical hydrogen evolution reaction: identification of sulfur atoms as catalytically active sites for H⁺ reduction, *ACS Catal.* 6 (2016) 7790–7798.
- [45] P.D. Tran, T.V. Tran, M. Orio, S. Torelli, Q.D. Truong, K. Nayuki, Y. Sasaki, S.Y. Chiam, R. Yi, I. Honma, J. Barber, V. Artero, Coordination polymer structure and revisited hydrogen evolution catalytic mechanism for amorphous molybdenum sulfide, *Nat. Mater.* 15 (2016) 640–646.
- [46] A.Y. Lu, X. Yang, C.C. Tseng, S. Min, S.H. Lin, C.L. Hsu, H. Li, H. Idriss, J.L. Kuo, K.W. Huang, L.J. Li, High-sulfur-vacancy amorphous molybdenum sulfide as a high current electrocatalyst in hydrogen evolution, *Small* 12 (2016) 5530–5537.
- [47] J. Benson, M. Li, S. Wang, P. Wang, P. Papakonstantinou, Electrocatalytic hydrogen evolution reaction on edges of a few layer molybdenum disulfide nanodots, *ACS Appl. Mater. Interfaces* 7 (2015) 14113–14122.
- [48] D. Gopalakrishnan, D. Damien, M.M. Shajumon, MoS₂ quantum dot-interspersed exfoliated MoS₂ nanosheets, *ACS Nano* 8 (2014) 5297–5303.
- [49] S. Bae, N. Sugiyama, T. Matsuo, H. Raebiger, K.-i. Shudo, K. Ohno, Defect-induced vibration modes of Ar+-irradiated MoS₂, *Phys. Rev. Appl.* 7 (2017).
- [50] K. Wu, Z. Li, J. Tang, X. Lv, H. Wang, R. Luo, P. Liu, L. Qian, S. Zhang, S. Yuan, Controllable defects implantation in MoS₂ grown by chemical vapor deposition for photoluminescence enhancement, *Nano Res.* 11 (2018) 4123–4132.